Sticky orbits of a kicked harmonic oscillator

2005 J. Phys.: Conf. Ser. 7 68

(http://iopscience.iop.org/1742-6596/7/1/006)

Institute of Physics Publishing
doi:10.1088/1742-6596/7/1/006

Sticky orbits of a kicked harmonic oscillator

J. H. Lowenstein

Dept. of Physics, New York University, New York, NY 10003, USA

E-mail: john.lowenstein@nyu.edu

Abstract. We study a Hamiltonian dynamical system consisting of a one-dimensional harmonic oscillator kicked impulsively in 4:1 resonance with its natural frequency, with the amplitude of the kick proportional to a sawtooth function of position. For special values of the coupling parameter, the dynamical map W relating the phase-space coordinates just prior to each kick acts locally as a piecewise affine map K on a square with rational rotation number p/q. For $\lambda = 2\cos 2\pi p/q$ a quadratic irrational, a recursive return-map structure allows us to completely characterize the orbits of the map K. The aperiodic orbits of this system are sticky in the sense that they spend all of their time wandering pseudo-chaotically (with strictly zero Lyapunov exponent) in the vicinity of self-similar archipelagos of periodic islands. The same recursive structure used locally for K gives us the asymptotic scaling features of long orbits of W on the infinite plane. For some coupling parameters the orbits remain bounded, but for others the distance from the origin increases as a logarithm or power of the time. In the latter case, we find examples of sub-diffusive, diffusive, super-diffusive, and ballistic power-law behavior.

1. Introduction

One of the simplest models for studying chaotic transport in low-dimensional Hamiltonian dynamical systems is that of a one-dimensional harmonic oscillator kicked in 4:1 resonance with its natural frequency, with the amplitude of the kick a periodic function of position[1, 2]. The phase portrait of the dynamical map has the discrete translation symmetry of a square crystal lattice and, in the case of a sinusoidal kick function with coefficient of order unity, features a thin, connected chaotic layer – the stochastic web– extending to infinity (see Figs. 1 and 2). The asymptotic behavior of chaotic orbits in the stochastic web have been subjected to intensive numerical investigation. One of the more intriguing discoveries[3, 4] has been that of sticky orbits which spend long time intervals trapped in self-similar systems of islands of stability. If the islands themselves are accelerator modes, which proceed to infinity with a non-zero average velocity, the corresponding sticky orbits alternate between periods of trapping and rapid ballistic flights. For certain parameter values, the presence of sticky orbits has been found to give rise to asymptotic super-diffusive transport[5].

The present report is based on recent collaborative work with G. Poggiaspalla and F. Vivaldi (the interested reader can find a more detailed account in [6]). Our focus is a class of kicked-oscillator models with piecewise linear (sawtooth) kick functions, with parameter values chosen so that all aperiodic orbits are sticky in the sense described above. The model was proposed in [7] as a example of pseudochaos[8, 9], i.e. the generation of complex phase-space structure without exponential divergence of nearby trajectories.

The advantage of this particular choice of kick function is the simplicity of the dynamics: all orbits, both periodic and aperiodic, can be analyzed completely. The key here is the crystalline

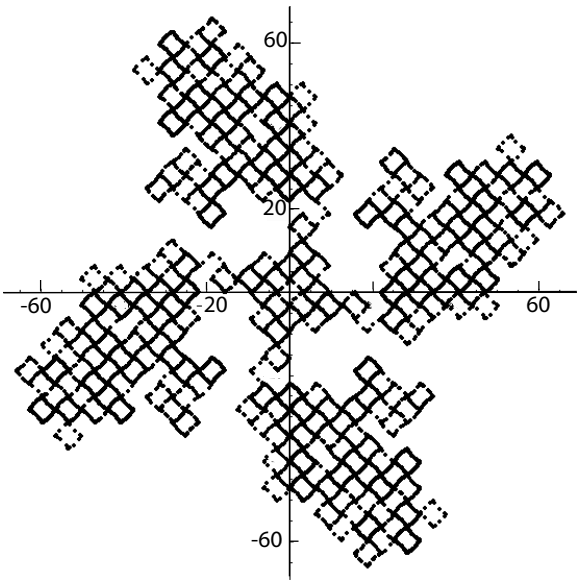

Figure 1. Stochastic web produced by 10000 iterations of the kicked-oscillator dynamical map with kick function $f(y) = 0.8 \sin y$.

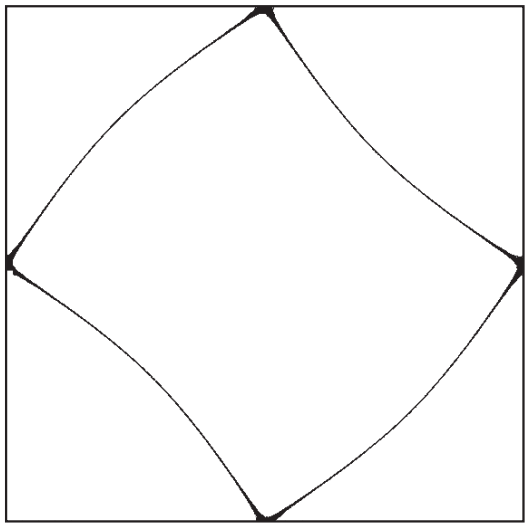

Figure 2. Same as in Fig. 1, but folded into the fundamental cell $[-\pi, \pi)^2$.

structure of the 2D phase space and the corresponding decomposition of the kicked-oscillator map W into a local part (a piecewise affine map on the square fundamental cell, with parameter-dependent rational rotation number) and and a global lattice transformation ($\pi/2$ rotation plus translation).

For the chosen class of models, the recursive return-map dynamics and resulting fractal geometry of the local map can be taken over completely from known results for piecewise rational rotations [10, 11, 12, 13, 14, 15, 16, 17, 18], and, with relatively little additional effort, extended to the full kicked-oscillator map. For the latter, self-similarity is governed by three scaling ratios, a temporal factor ω_T, a local spatial factor ω_K, and a global spatial factor ω_W. The first two determine the local fractal geometry, whereas ω_T and ω_W together determine the asymptotic long-time power-law behavior of orbits on the infinite plane.

As we shall see below, the asymptotic behavior depends crucially on the rotation number of the local dynamical map, varying over the full range of possibilities: in some cases the orbits are uniformly bounded, while in others the distance increases as $\log t$ or t^μ, with $\mu < \frac{1}{2}$ (sub-diffusive), $\mu = \frac{1}{2}$ (diffusive), $\frac{1}{2} < \mu < 1$ (super-diffusive), or $\mu = 1$ (ballistic). In all cases, the aperiodic orbits, apart from accelerator modes, are restricted to sets of zero Lebesgue measure.

2. Preliminaries

We start with he impulsively driven harmonic oscillator Hamiltonian

$$H(x, y, t) = \frac{1}{2}(y^2 + x^2) + F(y) \sum_n \delta(t - \frac{n\pi}{2})$$

with corresponding equations of motion

$$\dot{x} = y + f(y) \sum_n \delta(t - \frac{n\pi}{2}), \quad \dot{y} = -x,$$

where $f(y) = F'(y)$. Here y and $-x$ are proportional, respectively, to the usual position and momentum variables, and units are chosen so that the orbit in phase space consists of clockwise

circular arcs of angle $\pi/2$ alternating with y-dependent horizontal jumps, as in the example of Fig.3.

We define a dynamical map W linking the points (x, y) just prior to successive jumps:

$$W \begin{pmatrix} x \\ y \end{pmatrix} = \begin{pmatrix} 0 & 1 \\ -1 & 0 \end{pmatrix} \begin{pmatrix} x + f(y) \\ y \end{pmatrix} = \begin{pmatrix} y \\ -x - f(y) \end{pmatrix}.$$

Our choice of kick amplitude is the periodic, piecewise linear ("sawtooth") function

$$f(y) = \lambda\{y\}_\tau = f(y + \tau)$$

$$\{x\}_\tau \stackrel{\text{def}}{=} \{x/\tau\}\tau = x - \lfloor x \rfloor_\tau, \quad \lfloor x \rfloor_\tau \stackrel{\text{def}}{=} \lfloor x/\tau \rfloor \tau$$

where τ is a real, non-zero parameter which sets the scale in phase space, and

$$\lambda = 2\cos\frac{2\pi p}{q}, \quad p, q \in \mathbb{Z}.$$

The sawtooth kick function is shown in Fig. 6. It is easy to verify the invariance property

$$W \begin{pmatrix} x + m\tau \\ y + n\tau \end{pmatrix} = W \begin{pmatrix} x \\ y \end{pmatrix} + \begin{pmatrix} n\tau \\ -m\tau \end{pmatrix},$$

which endows the overall phase portrait with the crystalline symmetry of the square lattice $\tau\mathbb{Z}^2$. The fundamental cell of this lattice is Ω,equal to $[0, \tau)^2$ for $\tau > 0$, and to $(\tau, 0]^2$ for $\tau < 0$. For the example of Fig. 3, the first 100 iterations of the dynamical map W are shown in Fig. 4. When

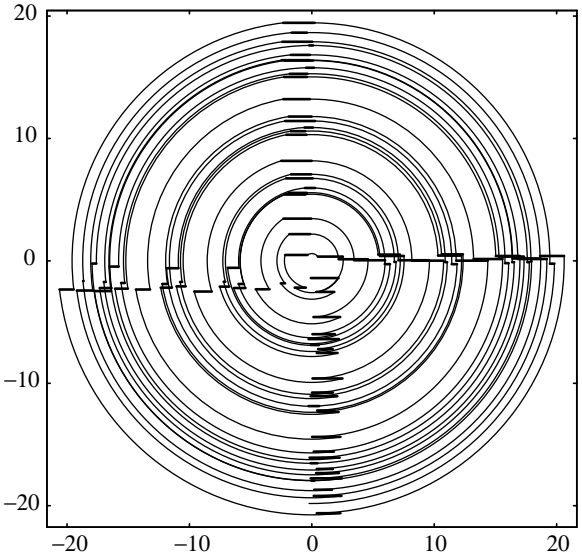

Figure 3. Kicked-oscillator orbit for sawtooth kick function $f(y) = \lambda\{y\}_\tau$, $\lambda = \tau = -\frac{1}{2}(1 + \sqrt{5})$. The kicks are drawn as horizontal segments linking the successive 90^o arcs of free oscillation. The first 25 oscillator periods (with 100 kicks) are shown.

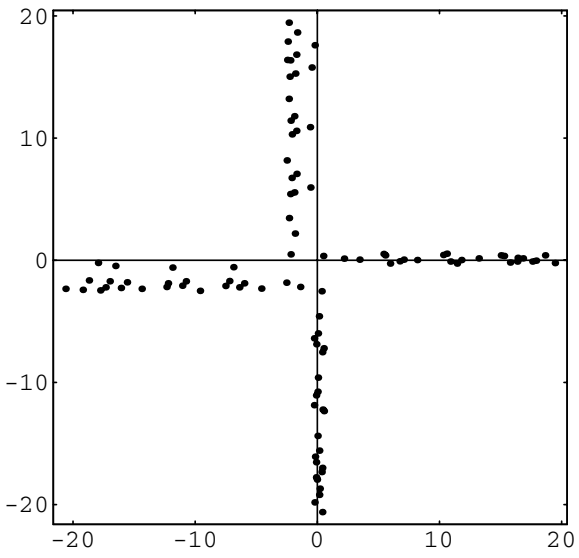

Figure 4. Orbit of dynamical map W, a stroboscopic view of the orbit of Fig. 3, in which one selects the point just preceding each kick. The orbit originates in Ω and moves outward along each axis with a non-zero average velocity.

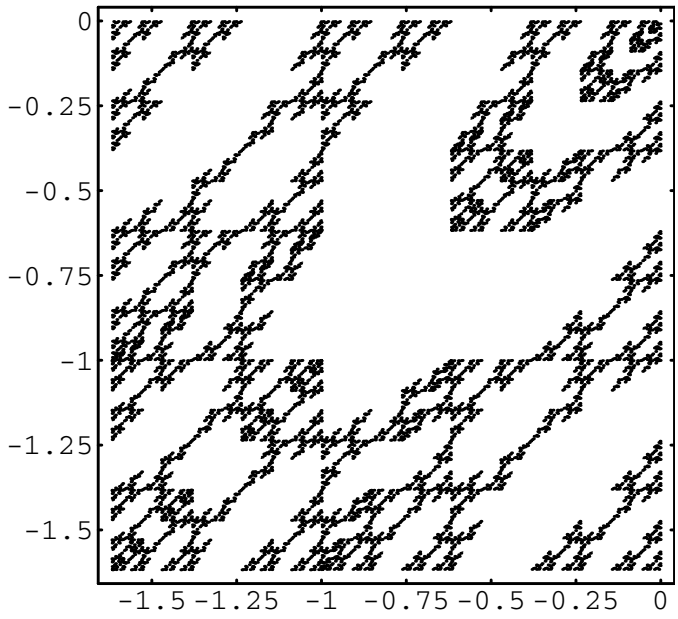

Figure 5. Same orbit as in Fig. 4 extended to 10000 iterations and folded into the fundamental cell $(\tau, 0]^2$ by $(x, y) \mapsto (\{x\}_\tau, \{y\}_\tau)$.

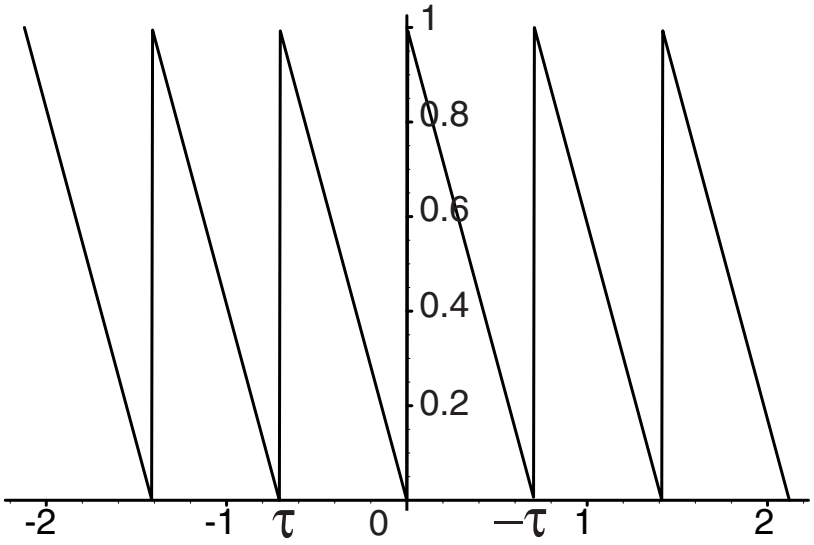

Figure 6. Sawtooth kick function $f(y)$ for $\lambda = 2\tau = -\sqrt{2}$.

extended to 10000 iterations and folded into the fundamental cell, the same orbit generates the complicated pattern (part of a fractal) shown in Fig. 5.

It is important to note that the map W naturally decomposes into two pieces, a map on Ω linearly equivalent to a rotation by $2\pi p/q$, and a lattice rotation by $\pi/2$. Any point in the plane

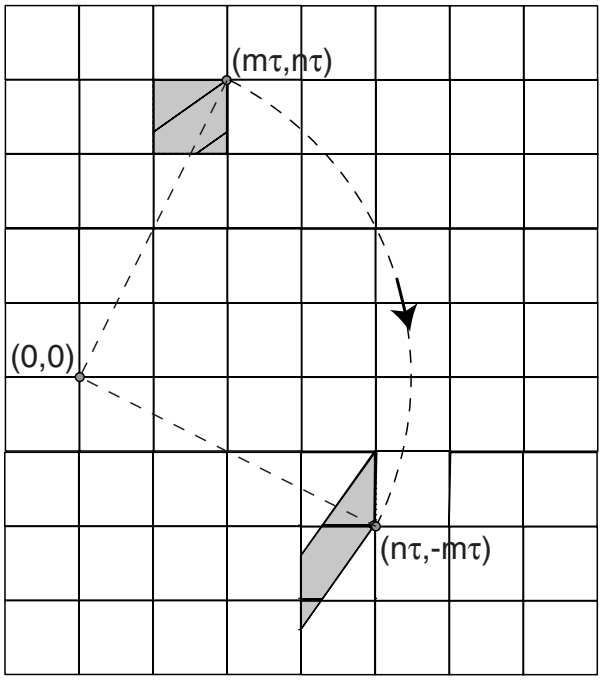

Figure 7. Action of the map W, for $\lambda = -\sqrt{2})$ on the fundamental cell translated by $(m\tau, n\tau)$, illustrating the decomposition (1).

can be written as $u + z$, with $u \in \Omega$ and $z \in \tau\mathbb{Z}^2$, with

$$W(u+z) = C \cdot u + F \cdot z, \tag{1}$$

$$C = \begin{pmatrix} 0 & 1 \\ -1 & -\lambda \end{pmatrix}, \quad F = \begin{pmatrix} 0 & 1 \\ -1 & 0 \end{pmatrix}.$$

Note

$$C^q = 1, \quad F^4 = 1.$$

The action of W is illustrated in Fig. 7.

It is useful to modify the decomposition of W, by means of a lattice translation, to force the local part to map Ω onto itself. Thus, for any $u = (x, y) \in \Omega, z \in \tau\mathbb{Z}^2$, we define (see Fig. 8)

$$K(u) = C \cdot u - \begin{pmatrix} 0 \\ \Delta(u) \end{pmatrix} = \begin{pmatrix} y \\ \{-x - \lambda y\}_\tau \end{pmatrix}, \quad \Delta(u) = \lfloor -x - \lambda y \rfloor_\tau,$$

so that

$$W(u+z) = K(u) + L_u(z),$$

where

$$L_u(z) = \left(F \cdot z + \begin{pmatrix} 0 \\ \Delta(u) \end{pmatrix} \right),$$

Now K is a piecewise affine map from Ω onto itself, while L_u is a Euclidean lattice transformation.

A final refinement is introduced by identifying the lattice $\tau\mathbb{Z}^2$ with the set of Gaussian integers $\mathbb{Z}[i]$ (complex numbers with integer real and imaginary parts) via

$$(m\tau, n\tau) \in \mathbb{Z}^2 \leftrightarrow n + m\, i \in \mathbb{Z}[i].$$

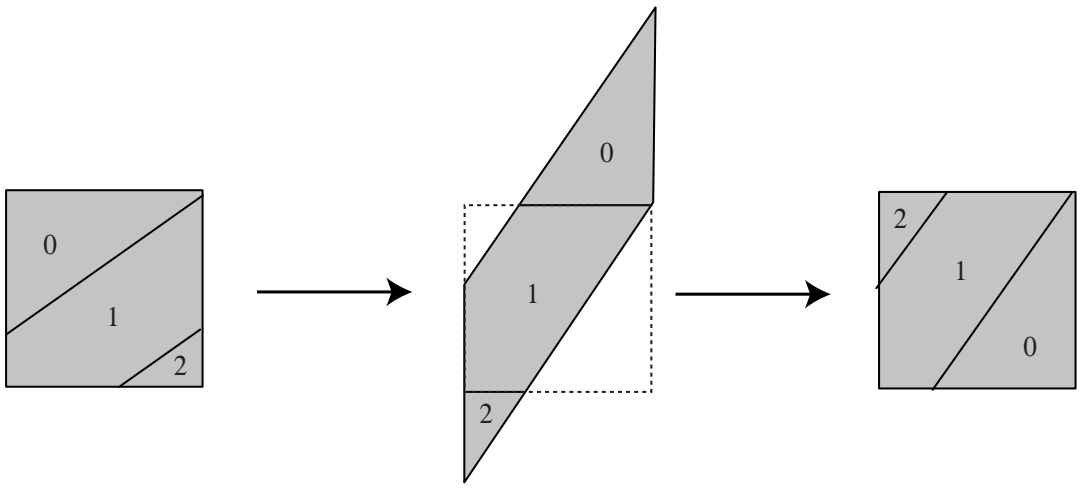

Figure 8. Action of the piecewise affine map K, for $\lambda = -\sqrt{2}$, viewed as a generalized rotation C followed by a translation by $(0, -\Delta(u))$, where $\Delta(u) = -\tau, 0, \tau$ for $u \in \Omega_0, \Omega_1, \Omega_2$, respectively.

and the plane $\mathbb{R}^2$ with $\Omega \times \mathbb{Z}[i]$. Elements of the latter will be written as $[u, \zeta]$. The map W becomes

$$W[u,\zeta] = [K(u), \Lambda_u(\zeta)], \quad \Lambda_u(\zeta) = i\zeta + \tau^{-1}\Delta(u) = i\zeta + \begin{cases} 1 & u \in \Omega_0 \\ 0 & u \in \Omega_1 \\ -1 & u \in \Omega_2 \end{cases} \tag{2}$$

with the domains Ω_j as in Fig. 8.

3. Self-similarity for K

For the cases of the parameter λ a quadratic irrational, i.e. a root of a quadratic polyniomial equation with integer coefficients, there are only eight distinct models, namely those with $\lambda = 1 \pm \sqrt{5}, -1 \pm \sqrt{5}, \pm\sqrt{2}, \pm\sqrt{3}$. Kouptsov, Lowenstein and Vivaldi[17] studied all of these cases systematically, together with one special example, with $\lambda = -\sqrt{2}$, for which the origin is located at the center of a square Ω of width 2τ. This model had been studied in some detail by Adler, Kitchens and Tresser[15].The treatment of [17] includes a complete classification of the orbits on the discontinuity set. When lifted to the plane, as orbits of W, these orbits will provide one of our most interesting examples, namely one (see Fig.20) with a super-diffusive long-time power law, generated by long spells of stickiness alternating with rapid flights.

Each quadratratic irrational model is characterized by at least one scaling sequence of nested triangles $\mathcal{D}(n) \subset \Omega, \quad n = 0, 1, 2, \ldots$, with the ratio of diameters $|\mathcal{D}(n+1)|/|\mathcal{D}(n)|$ equal to a spatial scale factor $\omega < 1$. The triangles tend in the limit $n \to \infty$ to a point u_∞: in coordinates with origin shifted to u_∞,

$$\mathcal{D}(L+1) = \omega \mathcal{D}(L) \tag{3}$$

The piecewise affine first-return maps $\rho(n)$ on $\mathcal{D}(n)$ also exhibit self-similarity, in the sense

$$\rho(L+1) = \omega \circ \rho(L) \circ \omega^{-1}.$$

Again we have placed u_∞ at the origin of coordinates. The map $\rho(n)$ partitions $\mathcal{D}(n)$ into convex polygons ("domains") $\mathcal{D}_j(n),\ j = 0, 1, \ldots, J-1$. Under iteration of $\rho(n-1),\ n > 0$, the images of $\mathcal{D}(n)$ visit the domains

$$\mathcal{D}_{p(j,0)}(n-1), \mathcal{D}_{p(j,1)}(n-1), \ldots, \mathcal{D}_{p(j,\nu_{j-1})}(n-1),$$

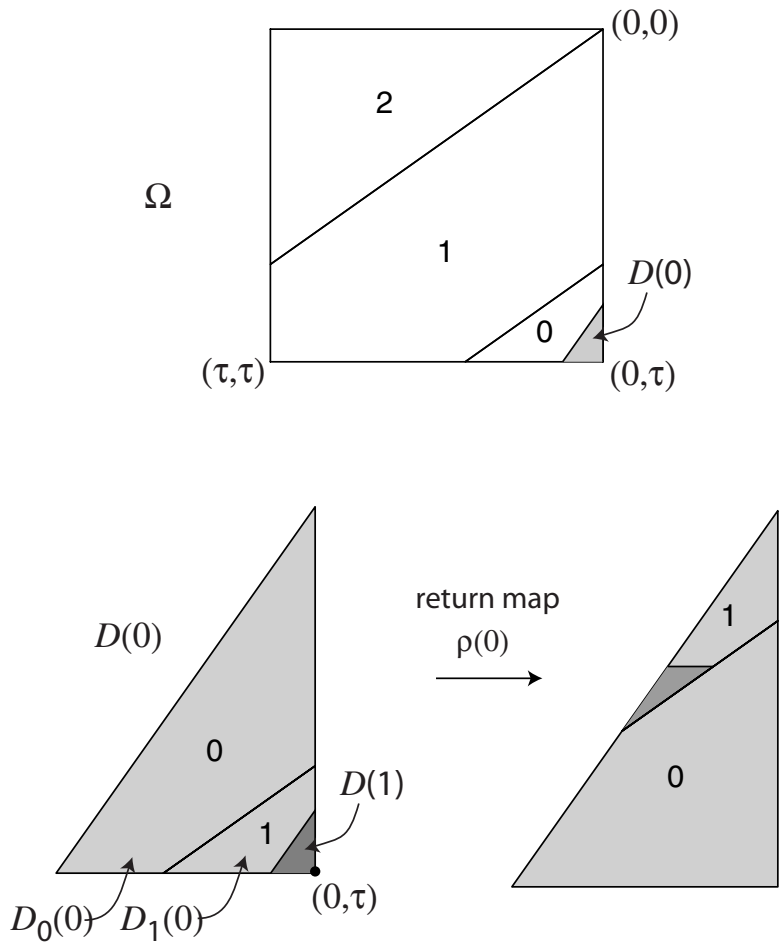

Figure 9. Scaling domains $\mathcal{D}(0)$ and $\mathcal{D}(1)$ for $\lambda = -\sqrt{2}$, showing the action of the first-return map $\rho(0)$ on thev subdomains $\mathcal{D}_0(0)$ and $\mathcal{D}_1(0)$. Relative to the limit point $u_\infty = (0, \tau)$, $\mathcal{D}(1) = \omega\mathcal{D}(0)$, with $\omega = 3 - 2\sqrt{2} \approx 0.172$.

returning to $\mathcal{D}(n)$, for the first time, on the ν_jth step. This return orbit is encoded by the *path* (sequence of indices)

$$p(j) = (p(j,0), p(j,1), \ldots, p(j,\nu_j - 1)) \tag{4}$$

For the lowest level, $n = 0$, we can also define a path function $p_0(j,t)$, where now j refers to the partition of Ω, and t counts iterations of K. Since it is not used in higher levels, the zeroth-level path function is not usually of great interest.

For the return maps, we have the recursion relation

$$\rho_j(L+1) = \rho_{p(j,\,\nu_j-1)}(L) \circ \cdots \circ \rho_{p(j,\,1)}(L) \circ \rho_{p(j,\,0)}(L).$$

It is assumed that $\mathcal{D}(n)$ fits entirely inside some $\mathcal{D}_j(n)$, and so $p(j,0)$ does not depend on j.

From the path function $p(j,t)$ we can calculate the *incidence matrix* A, with coefficients

$$A_{ji} = \#\{k : p(j,k) = i\} \quad i,j = 0,1,\ldots,J-1.$$

Here A_{ji} is the number of times that the $\rho(n-1)$-orbit of $\mathcal{D}_j(n)$ visits the domain $\mathcal{D}_i(n-1)$ before returning to $\mathcal{D}(n)$. This matrix governs the temporal scaling properties of the model.

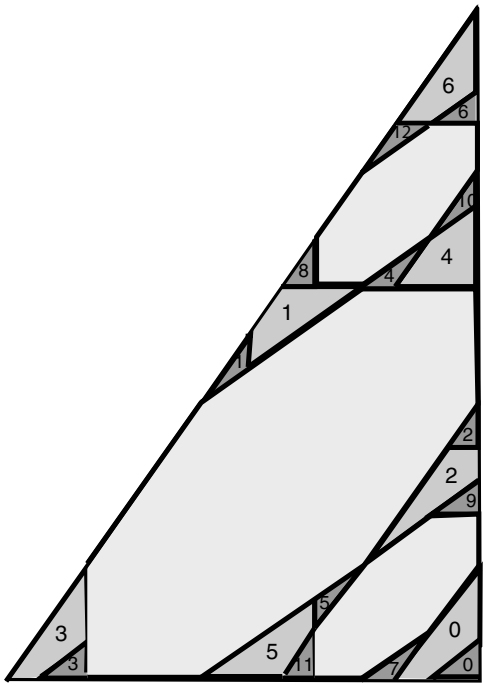

Figure 10. The $\rho(n)$ orbits of $\mathcal{D}_0(n)$ and $\mathcal{D}_1(n)$ in the scaling triangle $\mathcal{D}(n)$, for $\lambda = -\sqrt{2}$. The picture is the same for any n, thanks to scaling. We can read off the paths $p(j)$, $j = 0, 1$, namely $p(0) = (1, 0, 0, 0, 0, 1, 0)$, $p(1) = (1, 0, 0, 0, 0, 1, 0, 1, 0, 1, 0, 1, 0)$.

In particular, if $T_j(n)$ is the first-return time (iterations of K) of $\mathcal{D}_j(n)$, we have the recursion relation

$$T_j(L) = \sum_{k=0}^{\nu_j - 1} T_{p(j,k)}(L-1) = \sum_{i=0}^{J-1} A_{ji} T_i(L-1). \tag{5}$$

Asymptotically, the temporal scaling is governed by the largest eigenvalue ω_T of A.

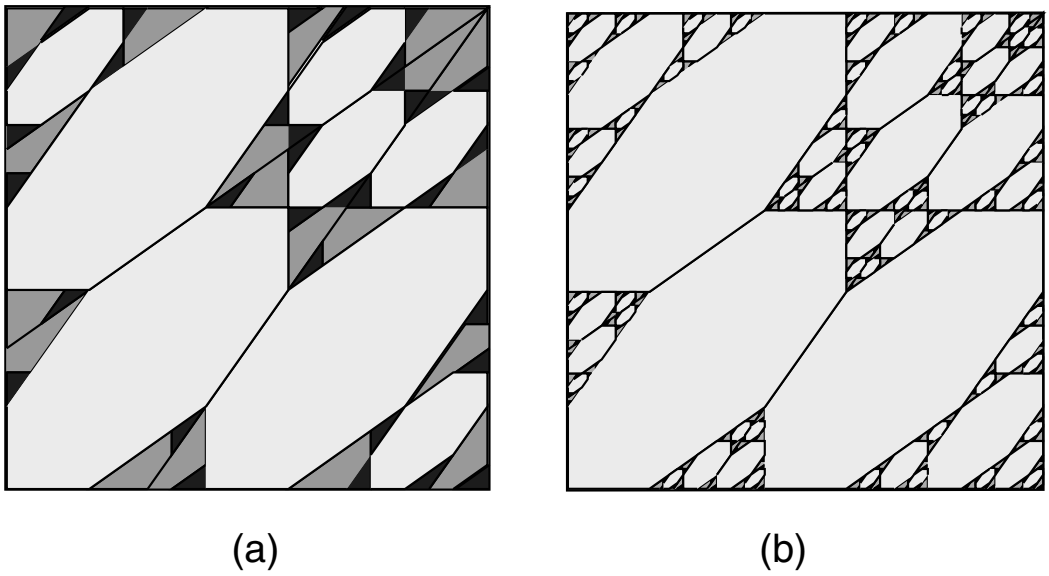

Figure 11. Tiling of Ω, up to a finite number of periodic domains and boundary lines, by first-return orbits of (a) $\mathcal{D}_j(0)$, $j = 0, 1$, and (b) $\mathcal{D}_j(1)$, $j = 0, 1$, for $\lambda = -\sqrt{2}$.

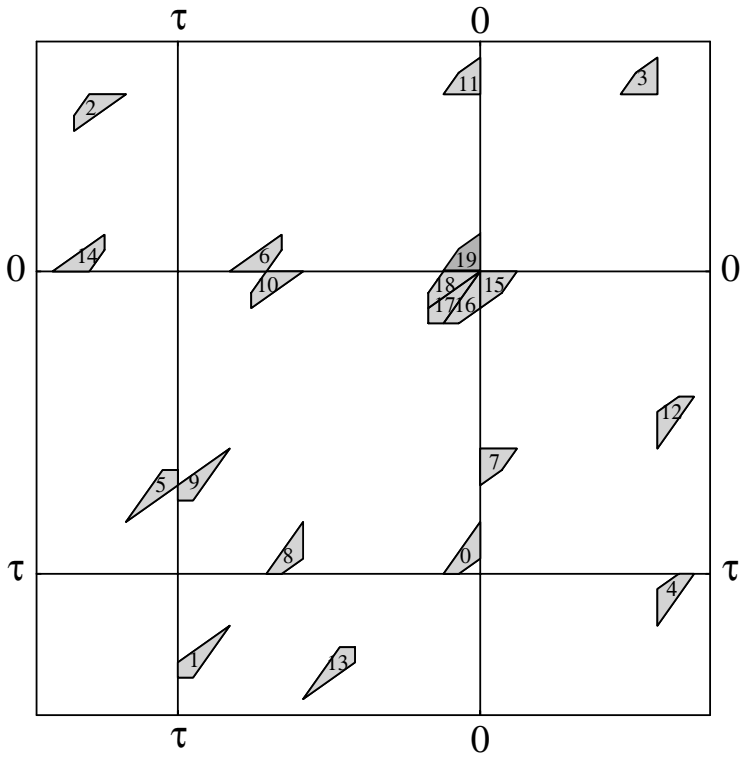

Figure 12. Lift to the plane of the first-return orbit of $\mathcal{D}_0(0)$, for $\lambda = -\sqrt{2}$.

In all of the known models with quadratic irrational λ, with one exception, there is a single scaling sequence of triangles satisfying the property of *recursive tiling*[18]: for any $n > 0$ and $m < n$, the $\rho(m)$ return orbits of all the domains $\mathcal{D}_j(n)$ tile $\mathcal{D}(m)$ up to a finite number of periodic domains. Moreover, for any $n > 0$, the K return orbits of all the domains $\mathcal{D}_j(n)$ tile Ω up to a finite number of periodic domains. Stictly speaking, the above statement ignores the boundaries of domains, but these can be included in the tiling as separate (lower-dimensional) domains [17]. The exceptional case is $\lambda = -\sqrt{3}$, where two disjoint scaling sequences, with different temporal scaling factors ω_T, are needed for a complete tiling.

For n tending to ∞, the fraction of Ω covered by the K return orbits of $\mathcal{D}_j(n)$ shrinks to zero, as more and more of the periodic domains are revealed (see Fig. 11). In the limit we are left with a (Lebesgue) measure-zero *residual set* of discontinuity-avoiding aperiodic orbits which are complementary to the set of all periodic domains (an example is shown in Fig. 5). The residual set is a fractal of (Hausdorff and box-counting) dimension $\log \omega_T / \log \omega$, which can be derived rigorously by exploiting the recursive structure [18].

A *tile* of level n is defined as

$$\mathcal{D}_j^{\mathbf{t}}(n) \stackrel{\text{def}}{=} K^{t_0} \circ \rho^{t_1}(0) \circ \rho^{t_2}(1) \circ \cdots \circ \rho^{t_n}(n-1)\mathcal{D}_j(n)$$

where $\mathbf{t} = (t_0, t_1, \ldots, t_n)$ and $\rho^t(n)$ is the t-th iterate of the level-n first-return map. To each tile $\mathcal{D}_j^{\mathbf{t}}(n)$ we associate a code (finite sequence of integer pairs)

$$((j_0, t_0), (j_1, t_1), \ldots, (j_n, t_n)), \quad 0 \le j_i \le J-1\}, \quad 0 \le t_i < \nu_{j_k},$$

with $j_n = j$ and all other j_i uniquely determined by

$$j_0 = p_0(j_1, t_1) \quad j_i = p(j_{i+1}, t_{i+1}), \quad i > 0. \tag{6}$$

A point of the residual set, residing in the intersection of countably many nested tiles, thus corresponds to an infinite symbol sequence.

$$((j_0,t_0),(j_1,t_1),\ldots,(j_i,t_i),\ldots).$$

The action of the map K on the residual set can be represented symbolically by a *Vershik map* [19, 20] defined as follows: if i is the smallest index k such that t_k is less than its maximum value, then

$$((j_0,t_0),(j_1,t_1),\ldots,(j_i,t_i),\ldots)\mapsto((j'_0,0),(j'_1 0),\ldots,(j'_{i-1},0),(j_i,t_i+1),(j_{i+1},t_{i+1}),\ldots\ldots), \quad (7)$$

where the j'_k are determined uniquely using the path conditions (6). In the exceptional case where all t_k are maximal, the successor symbol sequence has all members of the form $(j',0)$, $\quad j'=p(j,0)$, independent of j. The updating scheme (7) resembles a multi-register odometer, but is more complicated, since the size of the kth register is not fixed, but depends on the identity and reading of the next higher register. The Gregorian calendar (modified to extend to infinite times) provides an everyday example (the number of days in a month depends on *which* month within *which* kind of a year.

4. Extension to the global map

From (2) it is clear that the K-orbit of any point $u\in\Omega$ can be lifted uniquely to a W-orbit in $\Omega\times\mathbb{Z}[i]$. By iterating this equation $T_j(0)$ times starting at an arbitrary point of $\mathcal{D}_j(0)$, it is not difficult to see that the lift of the first-return map $\rho(0)$ takes the form

$$\rho_W(0)[\mathcal{D}_j(0),\,\zeta]\stackrel{\text{def}}{=}W^{T_j(0)}[\mathcal{D}_j(0),\zeta]=[\rho(0)\mathcal{D}_j(0),\,i^{T_j(0)}\,\zeta+d_j(0)] \quad (8)$$

where

$$d_j(0)=\sum_{t=1}^{T_j(0)-1} i^{T_j(0)-t}\Delta(K^t\mathcal{D}_j(0))/\tau.$$

That $d_j(0)$ is well defined depends on the fact that for $t<T_j(0)$, $K^t\mathcal{D}_j(0)$ does not intersect any discontinuity line, and so $\Delta(u)$ is constant over the whole domain.

We note that $\rho_W(0)$ is not a first-return map on the plane: there is no guarantee that an orbit starting in the fundamental cell returns to it after one K return time (or ever). The important thing is that the images of $\mathcal{D}_j(0)$ remains intact (i.e. no branching occurs) during $T_j(0)$ iterations of W, after which the final image domain resides in the level-zero triangle $\mathcal{D}(0)$ of some cell. This allows us to build up W-orbits of arbitrary length from the lifted return orbits.

For arbitrary level n, we can lift the first-return map as

$$\rho_W(n)[\mathcal{D}_j(n),\zeta]=W^{T_j(n)})[\mathcal{D}_j(n),\zeta],$$

and we have the recursion formula

$$\rho_{W,j}(n+1)=\rho_{W,p(j,\nu_j-1)}(n)\circ\cdots\circ\rho_{W,p(j,1)}(n)\circ\rho_{W,p(j,0)}(n),$$

where $\rho_{W,j}(n)$ is $\rho_W(n)$ restricted to $\mathcal{D}_j(n)$. This leads in a straightforward manner to

$$\rho_W(n)[\mathcal{D}_j(n),\,\zeta]=[\rho(n)\mathcal{D}_j(n),\,i^{T_j(n)}\,\zeta+d_j(n)],$$

where

$$d_j(n+1)=\sum_{k=0}^{J-1}c_k(p(j))\,d_k(n) \quad (9)$$

where, for any finite sequence $a = (a_0, a_1, \ldots, a_{\nu-1})$, $a_k \in \{0, 1, \ldots, J-1\}$, $\nu \in \mathbb{N}$, we define, for $n \geq 1$,

$$T(a) = \sum_{s=0}^{\nu-1} T_{a_s}(n) \bmod 4, \qquad c_j(a) = \sum_{s=0}^{\nu-1} \delta_{j,a_s}\, i^{T(a_{s+1},\ldots,a_{\nu-1})} \tag{10}$$

where δ is the Kronecker symbol. Here it is assumed that $T_j(n) \bmod 4$ is independent of n, which can be verified for all of the models being studied. In matrix notation, we can write

$$d(n+1) = M \cdot d(n),$$

with

$$M_{jk} = c_k(p(j)), \quad 0 \leq j, k < J. \tag{11}$$

The matrix M will obviously play a crucial role in understanding, where applicable, the asymptotic scaling of unbounded orbits of W. In particular, if M has an isolated maximal eigenvalue $\omega_W > 1$, we will have a scaling relation for the displacement vector $d(n) \in \mathbb{Z}[i]^J$,

$$d(n) = M^n \cdot d(0) = \omega_W^n\, \xi + O(\omega'^n) \tag{12}$$

where $\omega' < \omega$. If ξ does not vanish, this scaling relation serves as the basis for power law growth of unbounded orbits, as we shall see below.

5. Asymptotic long-time behavior

In the present report we restrict our attention to aperiodic orbits which have symbolic sequences with periodic tails. Such orbits are dense in the set of all aperiodic orbits and have the distinct advantage that one can explicitly calculate the initial point in closed form and iterate the map exactly using the arithmetic of algebraic numbers $m + n\tau$, $m, n \in \mathbb{Z}$.

In several of the models considered, the global recursion matrix M of (11) has no expanding eigenvalue and in fact all orbits in the residual set are bounded. In the case $\lambda = -\sqrt{2}$, for example, the 2D phase space decomposes into invariant quartets of "supertiles" (plus a single supertile containing the origin), each identical in structure to that of Fig. 13. On the other hand, stickiness does not always imply boundedness, as we can see in the example of Figs. 3 and 4.

To understand the mechanism underlying the different possible asymptotic long-time behaviors, let us consider the case of an aperiodic point $z_0 = [u_0, \zeta_0]$, with $u \in \Omega$ corresponding to a symbol sequence with tail $(j,t), (j,t), (j,t), \ldots$. The treatment of any eventually symbol sequence is completely analogous[6]. We write

$$z_0 = [((j_0, t_0), (j,t)^\infty), \zeta_0].$$

According to the Vershik updating rule (7), we can move rapidly along the orbit, skipping from one level to the next, as follows. First, we iterate W, $T_{J_0}(0) - t_0$ times, to reach the point

$$z_1 = [(j_1, 0), (j, t+1), (j,t)^\infty), \zeta_1],$$

where $j_1 = p(j, t+1)$. This is a point in $[\mathcal{D}_{j_1}(0), \zeta_1]$, and so we can now apply the level-0 first-return map $\rho_W(0)$, $\nu_j - t - 1$ times, following the path

$$p(j|t+1) \stackrel{\text{def}}{=} (p(j,t+1), p(j,t+2), \ldots, p(j,\nu_j - 1)),$$

to reach the point

$$z_2 = [(j_2, 0), (j_1, 0), (j, t+1), (j,t)^\infty), \zeta_2],$$

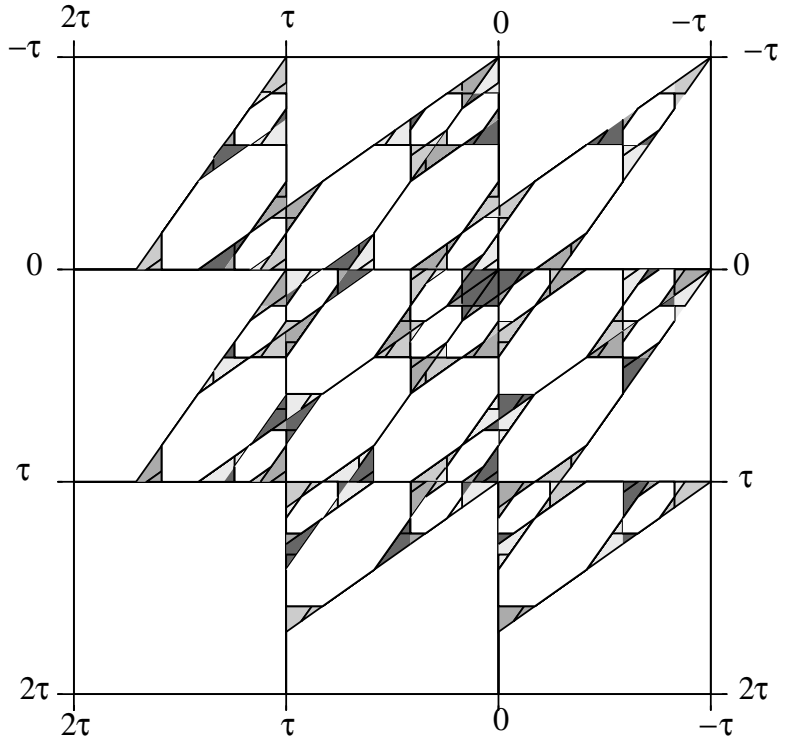

Figure 13. Supertile for $\lambda = -\sqrt{2}$. Any discontinuity-avoiding orbit initiated in this region remains there forever.

where $j_1 = p(j, t+1)$ and, in the notation of (10),

$$\zeta_2 = i^{T(p(j|t+1))}\zeta_1 + c(p(j|t+1)) \cdot d(0).$$

Now the point is in $[\mathcal{D}_{j_1}(1), \zeta_2]$ and we can apply $\rho_W(1)$, $\nu_j - t - 1$ times to reach

$$z_3 = [(j_2, 0), (j_2, 0), (j_1, 0), (j, t+1), (j, t)^\infty), \zeta_3],$$

with

$$\zeta_3 = i^{T(p(j|t+1))}\zeta_2 + c(p(j|t+1)) \cdot d(1).$$

Repeating the procedure produces an infinite sequence of points $z_0, z_1, z_2, \ldots$ with recursion relation

$$z_{n+1} = [u_{n+1}, \zeta_{n+1}] = [\rho(n)(u_n), i^{T(p(j|t+1))}\zeta_n + c(p(j|t+1)) \cdot d(n)]. \tag{13}$$

If the global recursion matrix M has a unique largest eigenvalue, then we have from (12)

$$c(p(j|t+1)) \cdot d(n) = c(p(j|t+1)) \cdot M^n \cdot d(0) \sim c(p(j|t+1)) \cdot \xi\, \omega_W^n.$$

If further $c(p(j|t+1)) \cdot \xi \neq 0$, the solution of (13), ζ_n, will have $O(\omega^n)$ growth for asymptotically large n. If we define the "time" t_n of z_n by $z_n = W^{t_n} z_0$, then

$$|\zeta_n| \sim t_n^\mu, \quad \mu = \frac{\log \omega_W}{\log \omega_T}.$$

Whether the power law is sub-diffusive, diffusive, or super-diffusive will depend on whether the square of ω_W is less than, equal to, or greater than ω_T, respectively. We have found examples of all these possibilities among the various models with quadratic irrational λ. It is straightforward to generalize the above discussion of asymptotic power law behavior to include symbol sequences with arbitrary periodicity, setting in at any level. The model with $\lambda = -\sqrt{3}$ boasts two disjoint scaling sequences of triangles (labeled A and B) tiling complementary parts of the residual set. The spatial scale factors on both sets are

$$\omega = 2 - \sqrt{3}, \quad \omega_W = 2,$$

but the temporal scaling is different:

$$\omega_T^{(A)} = 4, \quad \omega_T^{(B)} = 5.$$

This leads to different fractal dimensions, $\log \omega_T^{(A,B)} / \log \omega$, and also different asymptotic powers

$$\mu^{(A)} = \frac{1}{2}, \quad \mu^{(B)} = 0.430677...$$

In Fig. 14 we show one of the sub-diffusive B orbits, with initial point in Ω corresponding to a symbol sequence with periodic tail. The square of the distance from the origin is plotted vs. time on a log-log plot in Fig. 15. We verify the $t^{\mu^{(B)}}$ growth of the peak values in every cycle of the periodic symbol sequence, but also note the presence of numerous recurrences, i.e. returns to the fundamental cell. Making use of the hierarchy of return maps, we have succeeded in making a highly efficient search for recurrences of duration up to e^{50}. Fig. 16 gives a log-log plot of their relative frequency, revealing an interesting power law which we so far have been unable to explain.

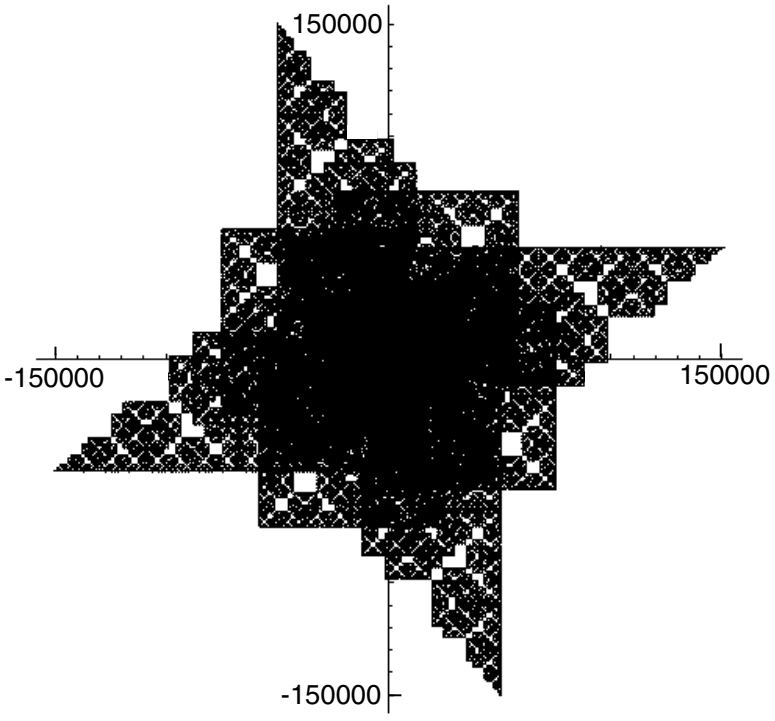

Figure 14. Orbit of a point in the residual set of Ω, for $\lambda = -\sqrt{3}$. The initial point is in the zero-level scaling triangle $[\mathcal{D}(0), 0]$ (sequence B), and the plotted points were obtained by iterating $\rho_W(0)$ 1438699 times.

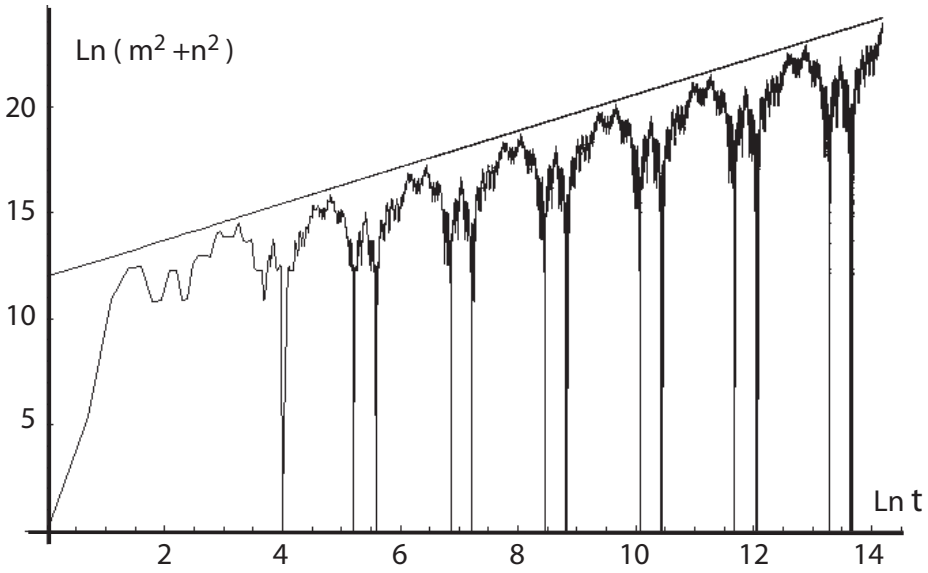

Figure 15. Log-log plot of the radial distance of each point of the orbit of Fig. 14 versus time. The straight line has a slope of $2\mu = \log 4/\log 5$.

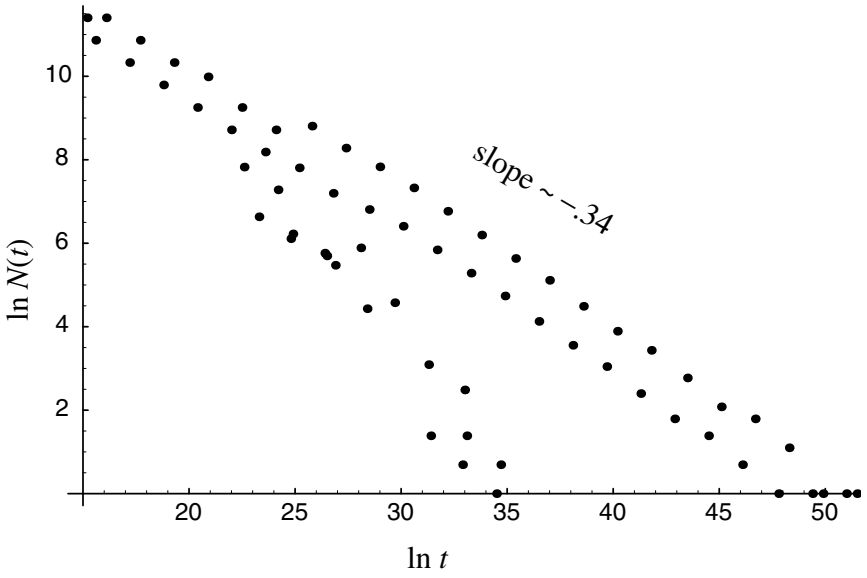

Figure 16. Log-log plot of the frequency of recurrences of the orbit of Figs. 14 and 15. Here $N(t)$ counts the number of recurrence times in a bin of size 0.1 on the $\ln t$ scale.

In addition to the models with the origin located at one corner of the fundamental cell, we have also studied one model with the origin at the center of a square of width 2τ. This is the case $\lambda = -\sqrt{2}$, for which the analysis of [17] makes it possible to include orbits in the discontinuity set as well as those in the residual set. Interestingly, the global scale factor ω_W is different for the two sets:

$$\omega_W^{(A)} = 1, \quad \omega_W^{(B)} = 5,$$

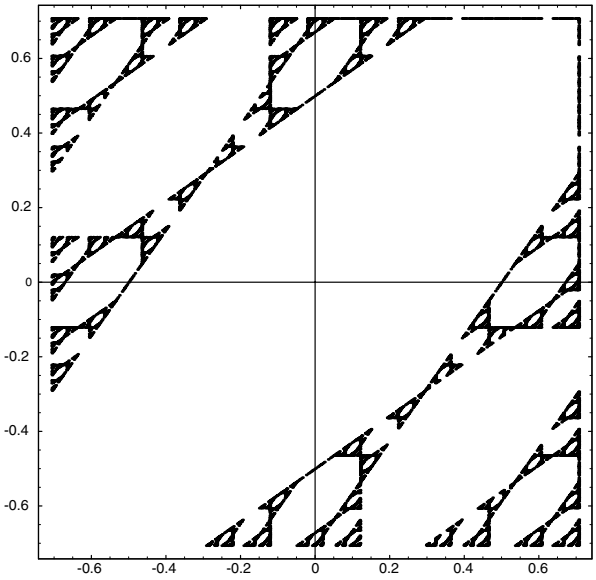

Figure 17. Orbit of K for $\lambda = -\sqrt{2}$ and centered origin, with $\Omega = (\tau, -\tau]^2$. The initial point is in the residual set and the map has been iterated 8000 times.

while $\omega = 3 - 2\sqrt{2}$ and $\omega_T = 9$ for both. The discontinuity-avoiding aperiodic orbits grow only logarithmically with time (see Figs. 18 and 19), while those starting on a discontinuity line have an interesting super-diffusive behavior, reminiscent of the sticky orbits found by Dana in the neighborhood of accelerator-mode islands in a genuine stochastic web[5]. Their intermittent outward spiralling is shown in Figs. 20 and 21.

A summary of the scaling properties for the models with quadratic irrational parameter which we have studied is given in the table.

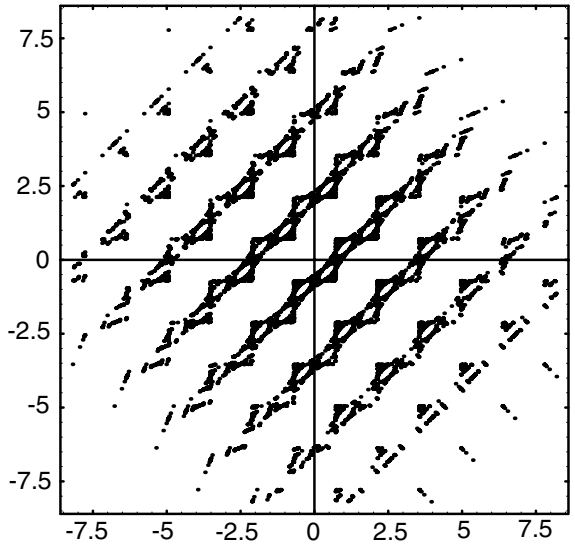

Figure 18. Same orbit as in Fig. 17,lifted to an orbit of W on the plane. With 10000 iterations, one sees no evidence of the orbit's slow drift to infinity (Fig. 19).

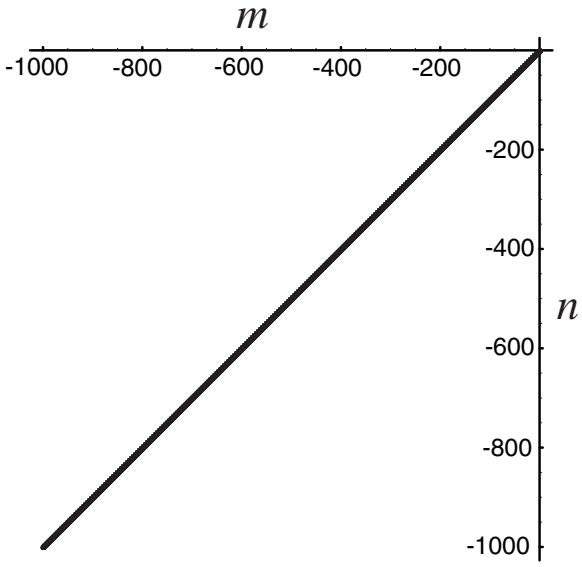

Figure 19. Same orbit as in Fig. 18, sampled uniformly on a logarithmic time scale and extending to times of order 10^{956}.

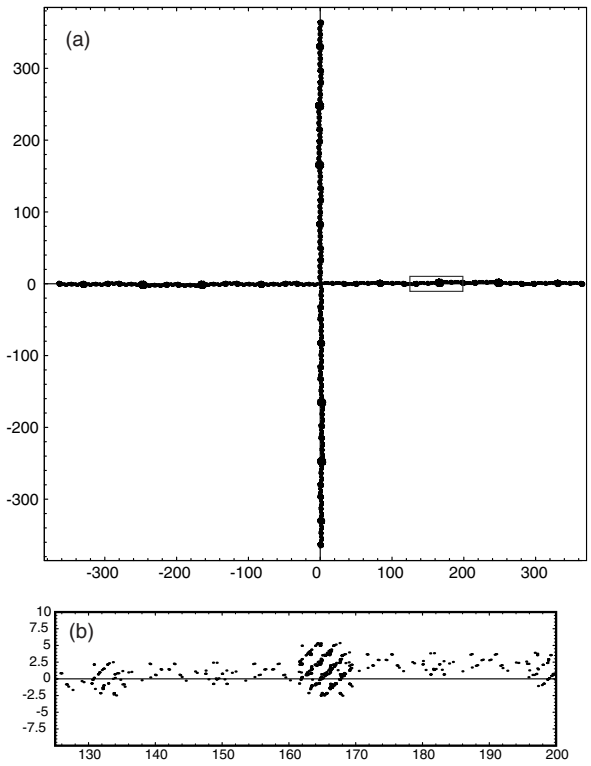

Figure 20. (a) Superdiffusive orbit in the model with $\lambda = -\sqrt{2}$, centered origin. The initial point is on the discontinuity set. (b) Detail of (a).

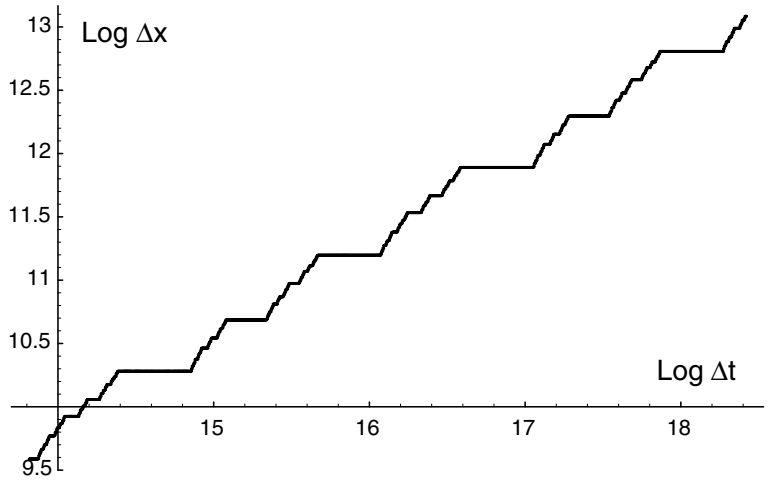

Figure 21. Log-log plot of the x coordinate versus the time for points of Fig. 20 near the x axis, selecting every fourth point of the W orbit. The plateaus represent long sojourns without significant forward movement, punctuated with rapid flights.

Table 1. Summary of local and global scaling parameters for the quadratic kicked-oscillator models.

λ	τ	ω	ω_T	ω_W	μ	behavior
$\sqrt{2}$	$\lambda/2$	$3-2\sqrt{2}$	9	1	0	bounded
$-\sqrt{2}$	$\lambda/2$	$3-2\sqrt{2}$	9	1	0	bounded
$(1+\sqrt{5})/2$	λ	$(3-\sqrt{5})/2$	4	1	0	bounded
$(1-\sqrt{5})/2$	λ	$(3-\sqrt{5})/2$	4	1	0	bounded
$(1+\sqrt{5})/2$	λ	$(3-\sqrt{5})/2$	4	4	1	ballistic
$(1+\sqrt{5})/2$	λ	$(3-\sqrt{5})/2$	4	4	1	ballistic
$\sqrt{3}$	$\lambda/3$	$7-4\sqrt{3}$	25	4	.430677	sub-diffusive
$-\sqrt{3}$(A)	$\lambda/3$	$2-\sqrt{3}$	4	2	.5	diffusive
$-\sqrt{3}$(B)	$\lambda/3$	$2-\sqrt{3}$	5	2	.430677	sub-diffusive
$-\sqrt{2}$(A)	$\lambda/2$	$3-2\sqrt{2}$	9	1	0	logarithmic
$-\sqrt{2}$(B)	$\lambda/2$	$3-2\sqrt{2}$	9	5	.732487	super-diffusive

Acknowledgements
I would like to thank G. Zaslavsky for helpful discussions. This research was supported in part by EPSRC grant No GR/S62802/01.

References

[1] G. M. Zaslavskii, R. Z. Sagdeev, D. A. Usikov, and A. A. Chernikov, *Weak chaos and quasiregular patterns*, Cambridge University Press, Cambridge (1991).
[2] G. M. Zaslavsky, *Physics of Chaos in Hamiltonian Systems* Imperial College Press, London (1998).
[3] G. M. Zaslavsky, M. Edelman, and B. A. Nyazov, Self-similarity, renormalization, and phase space nonuniformity of Hamiltonian chaotic dynamics, *Chaos* **7** (1997) 159–181.
[4] G. M. Zaslavsky and B. A. Nyazov, Fractional kinetics and accelerator modes, *Phys. Rep.* **283** (1997) 73–93.
[5] I. Dana, Global superdiffusion of weak chaos, *Phys. Rev. E* **69** (2004) 016212.
[6] J. H. Lowenstein, G. Poggiaspalla, and F. Vivaldi, Sticky orbits in a kicked-oscillator model, submitted to *Dynamical Systems*, (2004), preprint at http://www.maths.qmul.ac.uk/ fv/research/recentwork.html.
[7] O. Lyubomudrov, M. Edelman, and G. M. Zaslavsky, Pseudochaotic systems and their fractional kinetics, *Int. J. Mod. Phys B* **17** (2003) 4149–4167.
[8] G. M. Zaslavsky and M. Edelman, Weak mixing and anomalous kinetics along filamented surfaces, *Chaos* **11** (2001) 295–305.
[9] G. M. Zaslavsky and M. Edelman, Pseudochaos, *Perspectives and Problems in Nonlinear Science: a Celebratory Volume in Honor of Lawrence Sirovich*, eds. E. Kaplan, J. Marsden, and K. R. Sreenivasan, Springer, New York (2003) 421–423.
[10] A. Goetz, *Dynamics of piecewise isometries*, PhD Thesis, University of Chicago (1996).
[11] J. H. Lowenstein, S. Hatjispyros and F. Vivaldi, Quasi-periodicity, global stability and scaling in a model of Hamiltonian round-off, *Chaos* **7** (1997) 49–66.
[12] A. Goetz, Dynamics of a piecewise rotation, *Continuous and Discrete Dyn. Sys.* **4** (1998) 593–608.
[13] A. Goetz, Dynamics of piecewise isometries, *Illinois Journal of Mathematics* **44** (2000) 465–478.
[14] B. Kahng, Dynamics of symplectic piecewise affine elliptic rotation maps on tori, *Ergodic Theory and Dynamical Systems* **22** (2002) 483–505.
[15] R. Adler, B. Kitchens and C. Tresser, Dynamics of nonergodic piecewise affine maps of the torus, *Ergod. Th. and Dynam. Sys.* **21** (2001) 959–999.
[16] H. Bruin, A. Lambert, G. Poggiaspalla, S. Vaienti Numerical Investigations of a Discontinuous Rotation of the Torus, to appear in *Chaos* (2002).
[17] K. L. Kouptsov, J.H. Lowenstein and F. Vivaldi, Quadratic rational rotations of the torus and dual lattice maps, *Nonlinearity* **15** (2002) 1795–1482.

[18] J. H. Lowenstein, K. L. Kouptsov, and F. Vivaldi, Recursive tiling and geometry of piecewise rotations by $\pi/7$ *Nonlinearity* **17** 2004 1–25.
[19] A. M. Vershik, A theorem on the Markov periodical approximation in ergodic theory, *J.Sov. Math.* **28** (1985) 667–674
[20] G. Poggiaspalla, Self-similarity in piecewise isometric systems, preprint (2003).